ACS OMEGA

http://pubs.acs.org/journal/acsodf

Article

Sulfonation of Natural Carbonaceous Bentonite as a Low-Cost Acidic Catalyst for Effective Transesterification of Used Sunflower Oil into Diesel; Statistical Modeling and Kinetic Properties

Walaa A. Hassan, Ezzat A. Ahmed, Mohamed A. Moneim, Mohamed S. Shaban, Ahmed M. El-Sherbeeny, Nahid Siddiqui, Jae-Jin Shim, and Mostafa R. Abukhadra*

Cite This: *ACS Omega* 2021, 6, 31260−31271

Read Online

ACCESS | Metrics & More | Article Recommendations | Supporting Information

ABSTRACT: Bentonite sample enriched in organic matters (oil shale) was functionalized with $-SO_3H$ sulfonated carbonaceous bentonite (S-CB) by sulfonation process as a low-cost and effective acidic catalyst for the transesterification spent sunflower oil (SFO). The sulfonation effect was followed by several analytic techniques including X-ray diffraction, Fourier transform infrared, and scanning electron microscopy analysis. The catalytic performance of the sulfonated product was evaluated based on a statistical design which was built according to the response surface methodology and the central composite rotatable design. Using the S-CB acidic catalyst in the transesterification of spent SFO resulted in an actual biodiesel yield of 96% at studied conditions of 85 min at reaction interval, 50 °C as temperature,15:1 as methanol/oil ratio, and 3.5 wt % as S-CB loading. Moreover, the optimization function suggested enhancement to obtained yield up to 97.9% by selecting the values of temperature at 62 °C, the time at 98.5 min, the methanol/SFO ratio at 14.4:1, and S-CB loading at 3.4 wt %. The technical evaluation of the SFO biodiesel reflected the suitability of the product to be used as biofuels according to international standards. The kinetic behavior of the SFO transesterification reaction over S-CB is of pseudo-first order properties and of low activation energy. Finally, the synthetic S-CB as a solid acidic catalyst is of significant reusability and was reused five times with remarkable biodiesel yields.

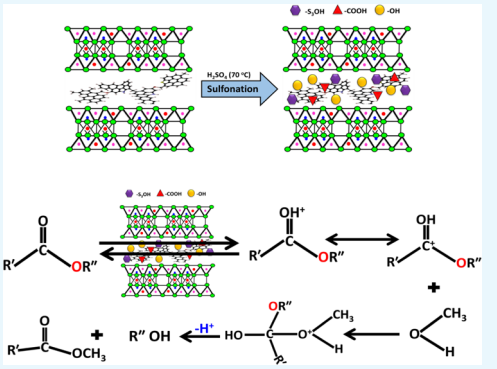

1. INTRODUCTION

Biodiesel and biofuels were addressed strongly as a clean and economic alternative solution for the traditional fuels that suffer from numerous environmental side effects.[1] The toxic emissions of fossil fuels direct the orientation of the researchers for such types of clean and environmental fuels as they are of low emissions (NOx, COx, and BTEX).[2,3] Technically, biodiesel is of significant viscosity, lubricity, cetane number, and flash point which qualifies it for direct use in engines or the formation of fuel blends.[4,5] Most of the produced biodiesels were derived from green resources (biomass and algae, vegetable-based oil, plant-based oil) and animal fats as series of fatty acid alkyl esters.[6] The spent cooking oil or the waste cooking oil [corn oil, sunflower oil (SFO), and palm oil] was introduced as commercial, recyclable, and low-cost precursors in the production of biodiesel by the transesterification reactions.[7] The alteration of such waste products into biodiesel through the transesterification or esterification reactions occurred in the existence of alcohol and a promising catalyst.[8] The heterogeneous catalysts that are of basic functional groups were reported as efficient materials of high reactivity, low cost, simple separation properties, high recyclability, effective mixing properties, and low hazardous byproducts.[9,10]

The acidic heterogeneous catalysts were evaluated widely for promising production of biodiesel as they are environmental products and can be applied effectively in the esterification as well as the transesterification reactions.[11,12] They were recommended to avoid the saponification effect of the commonly used basic catalyst during the reaction with the low-grade feed oils that contain a certain concentration of free fatty acids.[12] Several inorganic materials were evaluated as acidic catalysts by different acidification processes for the transesterification reactions including mesoporous silica, zeolite, montmorillonite, mica, and some metal oxides.[13−15] There are some drawbacks that were reported for the acidification of such inorganic materials including their low acidic densities, small pore sizes, high cost, and poor operational stability.[16] The acidic catalysts that were

Received: September 10, 2021
Accepted: November 8, 2021
Published: November 13, 2021

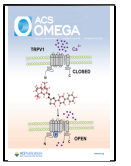

synthesized based on the carbonaceous and the different carbon materials are of high activity and significant thermal stability as compared to the acidified inorganic materials.[12,17] The low surface areas of such materials as well as their low hydrophilic surfaces are of strong influence in increasing the mass transfer resistance for the hydrophobic reactants which set limitations for the large-scale use of such catalysts.[17,18] Moreover, the structural properties of the carbon-based catalysts as amorphous materials increase the recovery difficulty for their particles from the treated oil samples.[17]

Several methods were studied to enhance the performance of the carbon-based acidic catalysts and to reduce the negative impacts of the previously reported drawbacks as their low surface area. This involved supporting the carbonaceous or the carbon materials into suitable carriers of high surface area or template the product by nanoporous materials.[17,18] Bentonite was investigated in several studies as one of the most effective low-cost carriers for the catalysts.[19] It is natural clay and composed essentially of smectite clay minerals with their unique technical properties as the flexible chemical structure, high adsorption capacity, high hydrophilic properties, high surface area, high natural reserves, and the high environmental value.[20−22] Bentonite can be found in nature in different forms related to the types of the dominant smectite mineral, the types of the present impurities, and the percentage of the present impurities.[20] The carbonaceous forms or organic-rich forms of bentonite (oil shale) were reported in nature in significant reserves and did not receive considerable studies about its qualification as a precursor for acidic heterogeneous catalysts. The carbonaceous form of bentonite is of organic/inorganic hybrid properties as it composed of laminated clay layers intercalated with organic matter that are commonly soluble forms of bitumen and insoluble kerogen.[23,24] Therefore, it was expected that the possible acidifications or sulfonation for it will result in a promising catalyst in which the sulfonated carbonaceous materials supported within the layers of bentonite that is of very high surface area and significant hydrophilic properties. Moreover, the catalyst will possess complex properties including sulfonated organic and inorganic components which will be of different catalytic behaviors and expected high activity.

The introduced study involved for the first time the catalytic activities of the sulfonated natural carbonaceous bentonite (oil shale) (CB) as a potential acidic catalyst in the transesterification of SFO into biodiesel. All the conducted transesterification tests were performed considering the suggested conditions by a statistical design which was built based on the response surface methodology (RSM) and central composite rotatable design (CCRD). Additionally, the kinetic and the thermodynamic behaviors of sulfonated carbonaceous bentonite (S-CB) were assessed in detail.

2. RESULTS AND DISCUSSION

2.1. Characterization of the Catalyst. *2.1.1. X-ray Diffraction Analysis.* The X-ray diffraction (XRD) patterns of normal bentonite (NB), CB, the prepared S-CB catalyst, and the spent S-CB catalysts are presented in Figure 1. The pattern of the NB shows the characteristic peaks of montmorillonite as the essential components at 6.55° (002), 19.85° (020), and 25.1° (105) (card nos: 00-003-0010 and 00-058-2010) (Figure 1A). The essential impurities which were detected with the NB sample are quartz and kaolinite. The crystal studies reflect the formation of NB with a crystallite size of 12.9 nm and basal

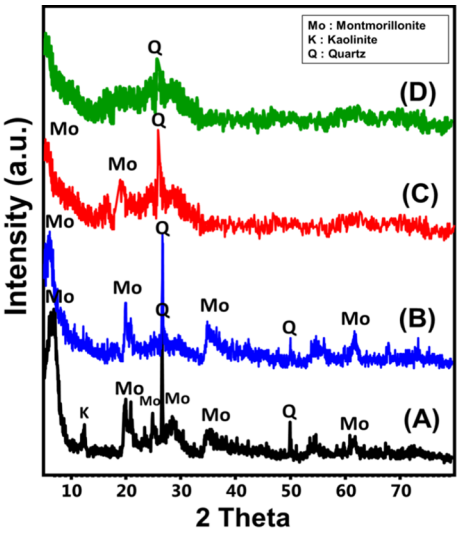

Figure 1. XRD patterns of NB sample (A), CB sample (B), S-CB product (C), and the spent S-CB catalyst after the transesterification tests (D).

spacing of 13.48 Å. The XRD analysis of the CB in comparison with the NB sample reflects a similar XRD pattern with observable deviation for the montmorillonite peaks to lower positions (6.05 and 19.77°) demonstrating expected distortion for its structural units (Figure 1B). This distortion might be related to the intercalated organic matters and this assumption can be supported by the significant increase in the basal spacing up to 14.59 Å as well as the average crystallite size that increased to 18.3 nm as compared to the obtained values for the NB sample.

After the sulfonation effect, the obtained pattern of CB emphasizes a strong reduction in the intensities of the identification peaks of montmorillonite reflecting strong structural influence for the H_2SO_4 acid (Figure 1C). The high acidic conditions are of strong leaching properties for the structural Al, Si, and Mg ions form the octahedral as well as the tetrahedral units which might cause a collapse for the sheet structure of montmorillonite.[25] Additionally, such strong acids cause a strong break for the C−O−C binding within the structure of the carbonaceous material and increase their amorphization degree.[13,18]

After the transesterification experiments, the pattern of the spent S-CB catalyst shows no significant changes in the observed diffraction peaks for the fresh catalyst except the reduction in the intensities of the peaks that might be related to the adsorbed glycerol or fatty acids on the surface of S-CB catalyst (Figure 1D).

2.1.2. Petrographic and Scanning Electron Microscopy Analyses. The inspection of the CB samples as thin sections under the transmitted microscope reflected their formation in a compacted lamination form (Figure S1). The samples showed very fine clay matrix with numerous impurities and the organic matters were observed extensively in the samples as a filamentous mat structure of brownish color (Figure S1).

The scanning electron microscopy (SEM) image of the raw CB demonstrates its morphology as massive particles of compacted irregular layers and this was detected widely for the clay particles (Figure 2A). Some samples show wide distribution for disseminated spherical grains on the surface of the clay particles which might be related to the present

https://doi.org/10.1021/acsomega.1c05021
ACS Omega 2021, 6, 31260−31271

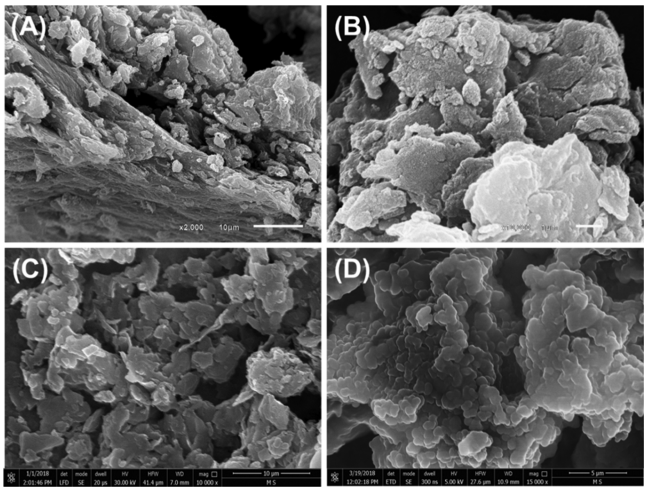

Figure 2. SEM images of raw CB (A), high magnification for the disseminated organic maters on the surface of CB particles (B), the smooth surface of CB particles after the sulfonation process (S-CB) (C), and high magnification for the rugged topography of S-CB (D).

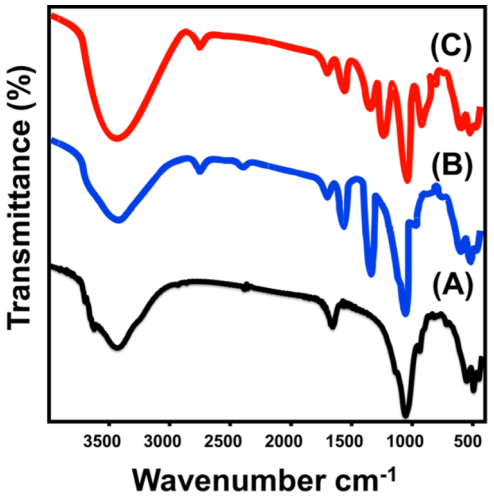

Figure 3. FT-IR spectra of NB (A), CB (B), and synthetic S-CB (C).

organic matters (Figure 2A,B). After the sulfonation process using H_2SO_4, the surface of the clay particles (S-CB) appear to be smoother than the particles of CB which might be related to the effect of the acid in dissolving the present impurities and oxidizing the organic matters (Figure 2C). However, the surface of the clay particles is smooth, the dissolving of the present impurities gives the product general morphology of enhanced porosity and irregular topography (Figure 2D). This will be of strong influence in enhancing the surface area and exposure for the active acidic sites which in turn will induce the catalytic activity of the S-CB as a solid acidic catalyst. The SEM of the used S-CB catalyst, demonstrate slight changes in the morphology (Figure S2). The particle of S-CB appeared to be stacked with massive and irregular grains which might be adsorbed glycerol molecules.

The measured surface area of CB, S-CB, and spent S-CB are 54.2, 61.3, and 58.7 m^2/g, respectively. The measured pore volumes are of CB, S-CB, and spent S-CB are 0.0489, 0.0542, and 0.0516 cm^3/g, respectively and the determined pore diameters are 3.11 nm (CB), 3.74 m^2/g (S-CB), and 3.22 m^2/g (spent S-CB). The increase in the surface area and porous properties after the sulfonation process is related to the effect of the acid in the removal of the associated impurities. The detected declination in the surface area and the pore volume of the used catalyst (spent S-CB) as compared to the fresh catalyst reflect the effect of the adsorbed glycerol and fatty acids in blocking the open pores.

2.1.3. Fourier Transform Infrared and Chemical Analysis. The Fourier transform infrared (FT-IR) spectra of NB, CB, and S-CB catalysts were used to follow the differences in the chemical structures of the different products (Figure 3). The spectrum of NB shows the common bands of essential chemical groups of montmorillonite mineral as the OH and/or H−O−H bending (3100−3700 cm^{-1}), the interlayer water (1640.6 cm^{-1}), Si−O stretching (1000.3 cm^{-1}), and Al−O stretching (918.2 cm^{-1}) in addition to the identification bands of Si−O−Mg, Fe−OH, and Si−O−Al bending vibration (400−1000 cm^{-1})[6,20] (Figure 3A). Regarding the spectrum of CB, it also shows the identification bands of the montmorillonite but at slightly deviated positions in addition to other bands related to the intercalated organic matters (Figure 3B). The identified organic chemical groups are the C−H stretching (2924.8 cm^{-1}), C═O stretching (1620 cm^{-1}), and CH or C−OH stretching (1428 cm^{-1})[26] (Figure 3B).

After the sulfonation process, the FT-IR spectrum of the S-CB catalyst demonstrates observable deviation for the previously reported bands for the montmorillonite mineral as well as the intercalated organic matters (Figure 3C). The increment in the wideness of the OH identification band related to the formation of COOH groups as a result of the incorporation of the acidic chemical groups within the structure of the intercalated organic matters under the oxidation effect of the sulfonation process.[13,27] The detection of absorption bands related to O═S═O vibration mode (1176.3 cm^{-1}) and $-SO_3H$ stretching (1008 cm^{-1}) groups confirm the successful sulfonation of the present organic matters and the incorporation of the sulfonated groups within their structures (Figure 3C).[13,27]

The elemental composition of CB, S-CB, and the spent S-CB catalysts were determined based on their EDX spectra. The raw CB composed of O (43.27%), Si (25.34%), Al (13.2%), C (9.53%), Fe (5.26%), K (0.93%), S (0.71%), Mg (0.66%), Cl (0.85%), and Na (0.23%). For the fresh S-CB catalyst, the determined elements are O (48.85%), Si (24.12%), Al (11.92%), C (6.41%), Fe (0.84%), K (0.63%), S (6.81%), Cl (0.22%), and Na (0.20%). The observed increases in the sulfur content reflected the successful sulfonation of the carbonaceous layers of bentonite.

The elemental composition of the catalyst after the transesterification tests are O (50.12%), Si (23.70%), Al (11.10%), C (8.31%), Fe (0.42%), K (0.51%), S (5.46%), Cl (0.322%), and Na (0.15%). The increase in the carbon content of the used S-CB as compared to the fresh catalyst might be related to the adsorbed glycerol. However, the declination in the sulfur content reflects the possible leaching of the $-SO_3H$ during the transesterification reactions. The acidity values of CB, S-CB, and spent CB are 0.34, 2.64, and 2.57 mmol/g, respectively.

2.2. Transesterification Results. *2.2.1. Validation of the Statistical Model.* The validation of the statistical design based on the selected illustrative model (second-order quadratic polynomial) was assessed considering the analysis results of the variance function (ANOVA). The statistical design which was

https://doi.org/10.1021/acsomega.1c05021
ACS Omega 2021, 6, 31260−31271

used to evaluate the catalytic performance of S-CB for the transesterification of spent SFO includes 26 tests which were suggested at different conditions considering the possible interaction between them [(A) temperature, (B) time, (C) methanol/SFO ratio, and (D) S-CB loading] (Table 1).

Table 1. Suggested Experimental Runs Based on the Statistical Design and the Measured Response (Biodiesel Yield)

std	run	temperature (°C) (A)	time (min) (B)	methanol ratio (%) (C)	S-CB loading (wt %)(D)	biodiesel yield (%) (Y)
6	1	75.00	20.00	15.00	2.00	79.3
17	2	25.00	85.00	9.50	3.50	83.3
11	3	25.00	150.00	4.00	5.00	71.9
22	4	50.00	85.00	15.00	3.50	96
10	5	75.00	20.00	4.00	5.00	69.9
7	6	25.00	150.00	15.00	2.00	78.8
8	7	75.00	150.00	15.00	2.00	89.3
12	8	75.00	150.00	4.00	5.00	79.9
23	9	50.00	85.00	9.50	2.00	83.7
24	10	50.00	85.00	9.50	5.00	87.7
25	11	50.00	85.00	9.50	3.50	90.3
4	12	75.00	150.00	4.00	2.00	75.6
15	13	25.00	150.00	15.00	5.00	83.5
20	14	50.00	150.00	9.50	3.50	87.3
16	15	75.00	150.00	15.00	5.00	93.2
5	16	25.00	20.00	15.00	2.00	71.3
3	17	25.00	150.00	4.00	2.00	66.2
13	18	25.00	20.00	15.00	5.00	75.2
1	19	25.00	20.00	4.00	2.00	54.6
26	20	50.00	85.00	9.50	3.50	90.3
21	21	50.00	85.00	4.00	3.50	83.5
18	22	75.00	85.00	9.50	3.50	91.9
9	23	25.00	20.00	4.00	5.00	58.3
2	24	75.00	20.00	4.00	2.00	65.8
19	25	50.00	20.00	9.50	3.50	81.3
14	26	75.00	20.00	15.00	5.00	84.3

Considering the high determination coefficient ($R^2 > 0.9$) for the fitting relations between the theoretically expected SFO based biodiesel yields and the experimentally determined values, the quadratic polynomial model is a significant model (Figure 4A). Therefore, it can be applied to describe the relationship between the studied parameters and the recognized biodiesel yields over the S-CB catalyst (Figure 4A). The predication deviation curve which was plotted for the conducted tests (26 tests) shows a regular distribution for the plotted deviation points from −1.64 to 1.89 considering the reference line as the base (Figure 4B). Also, the regression plot of the studentized residuals declares significant accuracy and normality for the polynomial model during the prediction of the influence of the factors as the inputs and the obtained SFO biodiesel yields as responses (Figure S3).

The analysis of ANOVA considering the values of model-*F*, model-Prob > *F*, and lack of fit, as well as the sum of squares, give valuable information about the validation of the polynomial model and the studied inputs (experimental factors) (Table 2). The model-*F* value (148.5) demonstrates the high significance properties of the used polynomial model and the noise effect did not exceed 0.01% (Table 2). The presented model-Prob-*F* parameters for all the affected factors are of values less than 0.05% which demonstrates the significance of them as experimental factors control the efficiency of the reactions. Moreover, these values suggest a nonlinear regression relation between the presented responses (biodiesel yield) and the assessed experimental factors as inputs (Table 2). The detect agreement between the values of the Pred *R*-squared (0.96), the Adj *R*-squared (0.98), and the Adeq precision (46.6) reflect adequate signals for all the conducted transesterification tests for SFO over S-CB catalyst and the significant value of the polynomial model to navigate the space of the used statistical design (Table 2).

Considering the reported results for the analysis of variances of the approaches and the recognized validation for the studied parameters and the illustrative polynomial model, the regression equation that describes the relationship between the responses (biodiesel yield) and the different studied factors [(A) temperature, (B) time, (C) methanol/SFO ratio, and (D) S-CB loading] can be represented by eq 1.

$$Y = +90.67 + 4.78 \times A + 4.76 \times B + 6.96 \times C + 2.18 \times D - 3.2 \times A^2 - 6.5 \times B^2 - 1.5 \times C^2 - 5.1 \times D^2 - 0.14 \times A \times B - 0.18 \times A \times C - 0.044 \times A \times D - 0.64 \times B \times C + 0.12 \times B \times D - 0.019 \times C \times D \quad (1)$$

2.2.2. Interaction Effect of the Essential Factors. 2.2.2.1. Reaction Time and Temperature. The influence of the assessed reaction time considering the impact of temper-

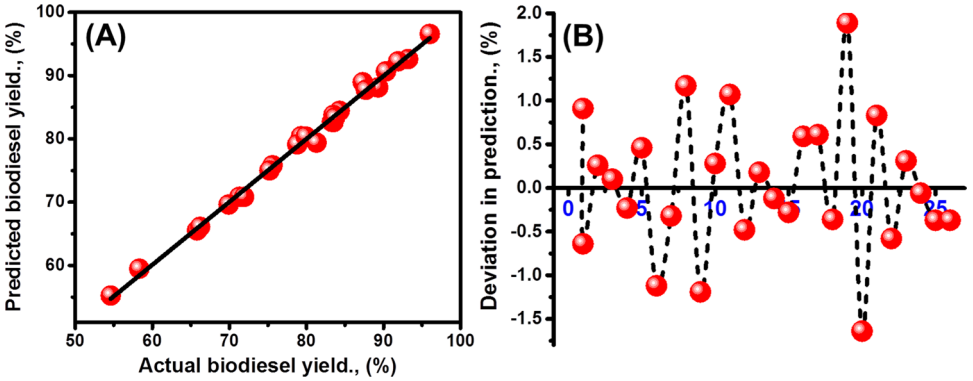

Figure 4. Correlation between the expected biodiesel yields and the determined yields (A) and the standard deviation of the expected biodiesel yields for the suggested 26 tests (B).

https://doi.org/10.1021/acsomega.1c05021
ACS Omega 2021, 6, 31260−31271

Table 2. ANOVA for the Studied Design (CCRD) Considering the Effective Parameters

source	sum of squares	DF	mean square	*F*-value	Prob > *F*	significantly
model	2830.95	14	202.21	148.55	<0.0001	significant
A	411.84	1	411.84	302.56	<0.0001	
B	408.03	1	408.03	299.75	<0.0001	
C	870.84	1	870.84	639.75	<0.0001	
D	85.80	1	85.80	63.04	<0.0001	
A^2	26.18	1	26.18	19.23	0.0011	
B^2	108.11	1	108.11	79.42	<0.0001	
C^2	2.81	1	2.81	2.06	0.01787	
D^2	66.54	1	66.54	48.88	<0.0001	
AB	0.33	1	0.33	0.24	0.0318	
AC	0.53	1	0.53	0.39	0.0470	
AD	0.031	1	0.031	0.022	0.0335	
BC	6.63	1	6.63	4.87	0.0495	
BD	0.23	1	0.23	0.17	0.0291	
CD	5.6×10^{-3}	1	5.62×10^{-3}	4.13×10^{-3}	0.0479	
residual	14.97	11	1.36			
lack of fit	14.97	10	1.50			
pure error	0.000	1	0.000			
cor total	2845.92	25				
std. dev.	1.17		*R*-squared	0.994		
mean	79.7		Adj *R*-squared	0.988		
C.V.	1.46		Pred *R*-squared	0.967		
press	92.99		Adeq precision	46.65		

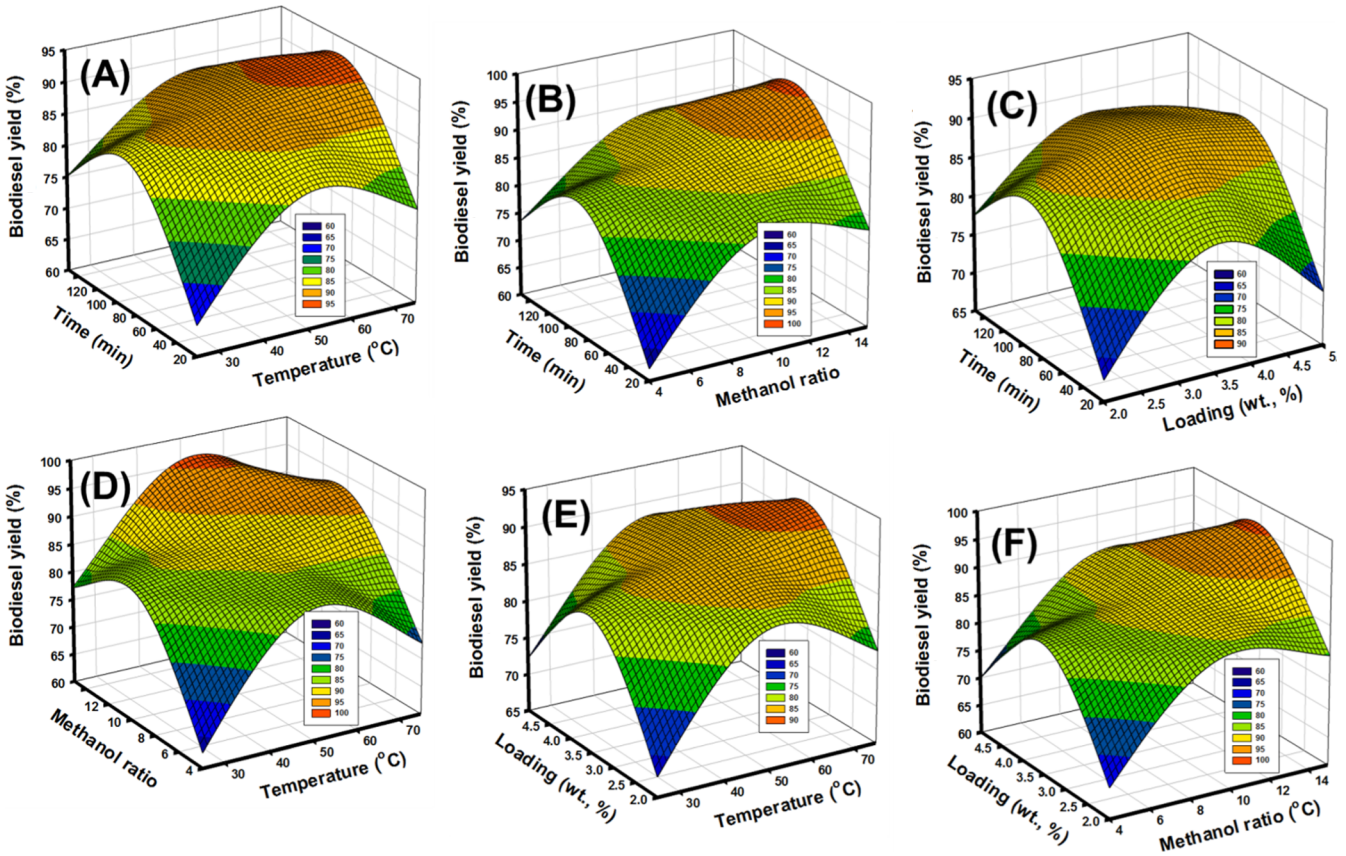

Figure 5. 3D curves or the interaction between the transesterification intervals and the temperature (A), between the transesterification intervals and the methanol content (B), between the transesterification intervals and the S-CB loading (C), the temperature and the methanol content (D), the temperature and the used S-CB loading (E), and the S-CB loading and the methanol content (F).

ature was evaluated after adjusting the other factors at an intermediate value [S-CB load (3.5 wt %) and methanol/SFO ratio (9.5/1)]. The observed 3D regression curve declared the interaction relation between both the interval and the temperature and its impact on the measured yields as responses (Figure 5A). Based on this 3D curve, the

https://doi.org/10.1021/acsomega.1c05021
ACS Omega 2021, 6, 31260−31271

performance of the S-CB catalyst demonstrates significant enhancement considering all the addressed values of temperature with the experimental expanding in the adjusted interval from 20 min up to 85 min. After that, the activity of S-CB declined slightly and the obtained yields decreased with the inspecting interval from 85 min up to 150 min (Figure 5A). Such declination in the S-CB catalytic activity catalyst after 85 min was assigned to the reported reversible behaviors of the transesterification systems as chemical reactions. After the equilibration reaction time, the formed FAME can be reintegrated in hydrolysis process converting them into their original fatty acids.[10] Therefore, the best conversion efficiency and the heist catalytic effect can be obtained after 85 min as a transesterification interval.

The observed positive interaction impact for the temperature values on the performance of the S-CB catalyst at 85 min appeared in enhancing the yields by 83.3, 90.3, and 91.9% after raising the temperature by 25, 50, and 75 °C, respectively (Figure 5A). This significant positive effect of the high temperature values was assigned to the exothermic properties of the transesterification processes. Therefore, the high temperature conditions promote the kinetic energy of the systems and in turn the resulted yields.[28,29] Moreover, the high temperature conditions are of significant role in decreasing the immiscibility, viscosity, mass transfer resistance between the different components which enhance the homogenization between them as well as the interaction chances.[1,30] Therefore, the best biodiesel yield from SFO was recognized after 85 min at 75 °C as temperature (91.9%).

2.2.2.2. Methanol/SFO Molar Ratio and Reaction Time. The impact of the conversion intervals considering the interaction effect of methanol/SFO molar ratio was inspected at intermediate values for the other factors [S-CB load (3.5 wt % g) and temperature (50 °C)]. The relation was presented in a 3D regression curve considering the resulted yields as the main response (Figure 5B). There is an observable positive interaction impact for the alcohol ratio on the catalytic performance of S-CB catalytic at all the inspected transesterification periods. This was detected clearly from the studied ratio of 4/1 (methanol/SFO ratio) up to 15/1 (methanol/SFO ratio) (Figure 5B). The incorporation of the used alcohol at a suitable molar ratio to the SFO preserves the reaction balance and causes significant reduction for the immiscibility properties and viscosity in addition to the mass transfer resistance.[5,30]

The positive impact for the interaction of the alcohol ratio at the best interval (85 min) appeared experimentally in the remarkable enhancement in the resulted SFO based yields over S-CB by 83.5, 90.3, and 96% at the alcohol molar ratios of 4/1, 9.5/1, and 15/1, respectively (Figure 5B). Therefore, 15/1 as the alcohol/SFO molar ratio is the optimum value in system to achieve the best biodiesel yield from SFO over S-CB catalyst.

2.2.2.3. S-CB Loading and Reaction Time. The impact of the conversion intervals considering the interaction effect of the S-CB loading was inspected at intermediate values for the other factors [methanol/SFO ratio (9.5/1) and temperature (50 °C)]. The relation was presented in 3D regression curve considering the resulted yields as the main response (Figure 5C). The individual trends in the 3D curve show a strong interaction impact for the loading values on the catalytic performance of S-CB at all the evaluated intervals from 2 wt % up to 3.5 wt % (Figure 5C). The higher loading of S-CB causes significant increase in the numbers of the exposed acidic catalytic sites and the interacted surface area which are vital properties to enhance the transesterification rates.[31,32] The applied loadings of S-CB which are higher than 3.5 wt % is of adverse effects on the process and the determined yields (Figure 5C). This was illustrated as a result of the oversuspension of the S-CB particles within the liquid phases which increases the viscosity as well as the mass transfer resistance.[10]

The positive impact for the interaction of the S-CB loading values at the best interval (85 min) appeared experimentally in the remarkable enhancement in the resulted SFO based yields 83.7% and 90.3% at studied loadings of 2, and 3.5 wt %, respectively (Figure 5C). Therefore, 3.5 wt % as the catalyst load is the optimum value in system to achieve the best biodiesel yield from SFO over the S-CB catalyst.

2.2.2.4. Temperature and Methanol/SFO Molar Ratio. The impact of the conversion temperature considering the interaction effect of methanol/SFO molar was inspected at intermediate values for the other factors [reaction time (85 min) and S-CB loading (3.5 wt %)]. The relation was presented in a 3D regression curve considering the resulted yields as the main response (Figure 5D). The catalytic effect as a function of the evaluated methanol/SFO molar ratio shows remarkable enhancement with operating the tests at high temperature conditions. At the lower limit of temperature (25 °C), the methanol ratios of 4/1, 9.5/1, and 15/1 resulted in SFO based yields of 74.5, 83.3, and 88.7%, respectively. At the intermediate limit (50 °C), the measured yields for the previous methanol molar ratios are 83.5, 90.3, and 96% in order. At the highest limit (75 °C), the methanol/SFO ratios of 4/1, 9.5/1, and 15/1 resulted in yields of 84.4, 91.9, and 96.5%, respectively. Moreover, the presented results emphasized the positive interaction impact for the methanol/SFO ratio on inducing the effect of temperature during the process. The maximum impact of the temperature was detected for the tests which involved methanol/SFO molar ratio of 15:1.

2.2.2.5. Temperature and S-CB Loading. The impact of the conversion temperature considering the interaction effect of the S-CB loading was inspected at intermediate values for the other factors [reaction time (85 min) and methanol/SFO ratio (9.5/1)]. The relation was presented in a 3D regression curve considering the resulted yields as the main response (Figure 5E). The catalytic effect as function of the evaluated S-CB loadings show remarkable enhancement with operating the tests at high temperature conditions. At the lower limit of temperature (25 °C), the used S-CB loadings of 2, 3.5, and 5 wt % resulted in SFO based yields of 75.3, 83.3, and 79.8%, respectively (Figure 5E). At the intermediate limit (50 °C), the measured yields for the previous loading values are 83.7, 90.3, and 87.7% in order. At the highest limit (75 °C), the S-CB loading of 2, 3.5, and 5 wt % induced the yields by 85.2, 91.9, and 89.3%, respectively (Figure 5E). The presented results also declared effective interaction impact for the S-CB loading value on enhancing the effect of temperature on the performance of the catalytic process. The maximum impact of the temperature was detected for the tests which involved 3.5 wt % of S-CB as catalyst loading.

2.2.2.6. Methanol/SFO Molar Ratio and S-CB Loading. The impact of the used methanol/SFO molar ratios considering the interaction effect of the S-CB loading was inspected at intermediate values for the other factors [reaction time (85 min) and temperature (50 °C)]. The relation was presented in a 3D regression curve considering the resulted yields as the main response (Figure 5F). At the lower limit of

https://doi.org/10.1021/acsomega.1c05021
ACS Omega 2021, 6, 31260−31271

Table 3. Suggested Best Solutions for the Transesterification of SFO over S-CB Catalyst

solution number	temperature (°C)	time (min)	methanol/oil ratio (%)	loading (wt %)	biodiesel yield (%)	desirability
1	69.4	88.7	14.9:1	3.77	98.6	1.000
2	65.4	107.44	14.5:1	4.33	98.03	1.000
3	62.2	120.7	14.26:1	3.68	97.9	1.000
4	65.4	97.5	14.3:1	4.38	97.6	1.000
5	55	104.5	13.2:1	3.85	96.7	1.000
6	57.7	125.4	13:1	3.83	96.3	1.000

S-CB loading (2 wt %), the used methanol/SFO molar ratios of 4/1, 9.5/1, and 15/1 resulted in SFO based yields of 75.3, 83.7, and 89.3%, respectively. At the intermediate value (3.5 wt %), the determined yields from SFO are 83.5, 90.3, and 96% for the previously present molar ratios in order. At the highest limit (5 wt %), the methanol/SFO molar ratios of 4/1, 9.5/1, and 15/1 induced the yields by 79.7, 87.7, and 93.6%, respectively.

2.2.3. Statistical Optimization. The optimization function of Design-Expert software as well as prediction option for the controlled quadratic polynomial programming were used to detected the theoretical solutions or suggestions for the best transesterification reactions of SFO over S.CB catalyst as presented in Table 3. The levels which were used during the predication processes were emphasized by the scheme constraints (Table S1). The actual best conditions which were detected experimentally ad resulted in biodiesel yield of 96% are 50 °C as temperature, 85 min as time, 15/1 as methanol/SFO ratio, and 3.5 wt % loading value. The suggested conditions based on the theoretical predictions can induce the yield up to 97.9% by adjusting the temperature at 62 °C, the time at 98.5 min, the methanol/SFO ratio at 14.4:1, and S-CB loading at 3.4 wt % (Table 3). Additionally, the yield can be enhanced up to 97.8% by adjusting the temperature at 53 °C, the time at 112.7 min, the methanol/SFO ratio at 15:1, and S-CB loading at 4 wt % (Table 3). Therefore, the catalytic effect of S-CB during the transesterification processes of SFO can be enhanced adjusting the experimental parameters at more suitable values.

2.2.4. Recyclability of the S-CB Catalyst. The used fractions of the S-CB catalyst (spent catalyst) after the accomplished transesterification experiments were washed with methanol for three runs as one of the recommended regeneration solvents. The washing runs consumed about 15 min and after the washing step, the sample was dried gently for 10 h at 70 °C and reused again in another transesterification test. Five reusability experiments of the S-CB catalyst, the conditions were adjusted at 85 min, 3.5 wt %, 15:1, and 75 °C for the reaction time, the S-CB loading, the methanol/SFO ratio, and the temperature, respectively (Figure 6). Based on the measured yields for the conducted five reusability tests, the S-CB catalyst is of promising stability and recyclability to be used effectively in the SFO transesterification process. The measured biodiesel yield is more than 95% for two reusing runs, than 93% for four runs, and then 90% for the evaluated five runs (Figure 6). The slight decrease in the measured yields from run 1 until run 5 might reflects the effect of the adsorbed glycerol on hindering the catalytic sites.[10]

2.3. Technical Properties. The physicochemical properties of the extracted biodiesel at the optimum conditions form SFO using S-CB catalysts were determined in comparison with the international standards (ASTM D-6751 and EN 14214) (Table 4). The measured density and viscosity values are

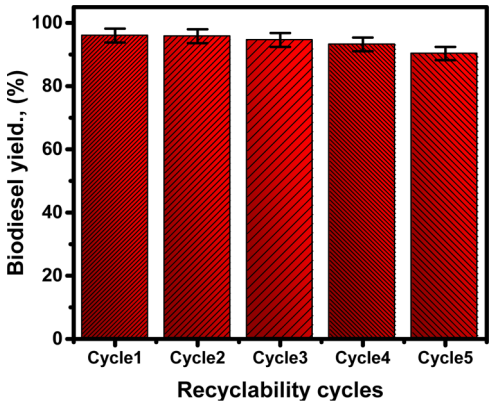

Figure 6. Obtained biodiesel yields for the studied five recyclability runs of S-CB as acidic catalyst.

Table 4. Technical and Physicochemical Properties of the Produced SFO Biodiesel Sample over S-CB as the Acidic Catalyst

contents	unit	ASTM D-6751	EN 14214	biodiesel
viscosity	mm^2/s	1.9−6	3.5−5	4.1
moisture content	wt (%)	<0.05	<0.05	0.032
flash point	°C	>93	>120	130.4
calorific value	MJ/kg		>32.9	43.7
cloud point	°C	−3 to 15		7.2
pour point	pp	−5 to 10		6.5
cetane number		≥47	≥51	55.6
density	g/cm^3	0.82−0.9	0.86−0.9	0.862
Na + K	mg/kg	≤5	≤5	4.6
acid value	Mg/KOH/g	≤0.5	≤0.5	0.33
iodine value			≤120	100.8

within the recommended international range for suitable biofuels. Moreover, the measured cetane index is higher than 45 which reflects the safety properties of the produced diesel to be used as fuel in the engines. Also, the measured flashpoint of the SFO based biodiesel is a suitable value for the safe handling and transportation of the produced biodiesel (Table 4).

2.4. Kinetic Studies. There are three steps that should be carried out during the transesterification of oil into biodiesel as declared by eqs 2−4. These equations emphasize the successive reaction of triglyceride (TG), diglyceride, and monoglyceride as the oil components with 1 mol of alcohol (methanol) to produce 1 mol of FAME which finally resulted in 3 mol of FAME and 1 mol of glycerol (GR) as presented in eq 6.[33] Based on the final equation of the reactions (eq 5), the rate of the transesterification process affected by the concentrations of TG and as well as the alcohol content.

$$\text{TG} + \text{methanol} \leftrightarrow \text{DG} + \text{ME} \quad (2)$$

https://doi.org/10.1021/acsomega.1c05021
ACS Omega 2021, 6, 31260−31271

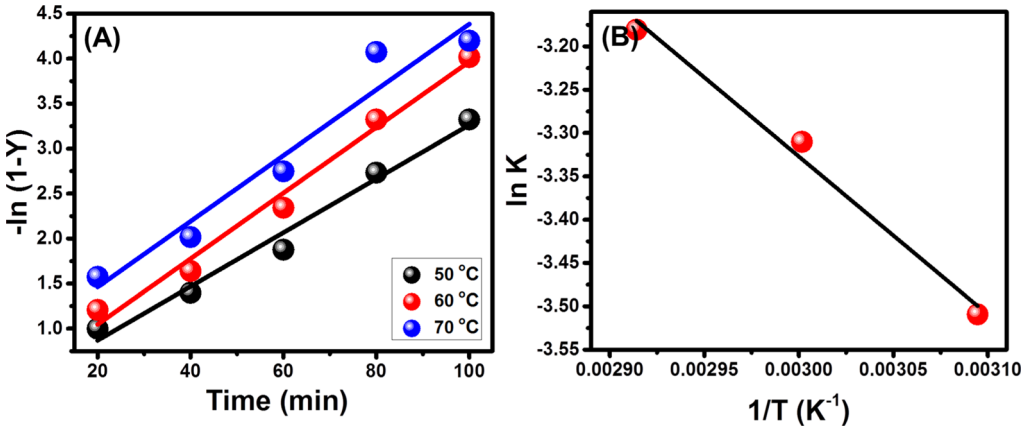

Figure 7. Linear regression plot of the transesterification results with pseudo-first order model (A) and Arrhenius plot ln k vs $1/T$ (B).

$$\text{DG} + \text{methanol} \leftrightarrow \text{MG} + \text{ME} \quad (3)$$

$$\text{MG} + \text{methanol} \leftrightarrow \text{GR} + \text{ME} \quad (4)$$

$$\text{TG} + 3\text{methanol} \leftrightarrow \text{GR} + 3\text{ME} \quad (5)$$

The transesterification process is of reversible behavior as chemical reaction; therefore, the presence of the alcohol molecules at suitable concentration is of a positive effect in directing to the forward side until the equilibrium.[31] However, the alcohol concentration is of no effect in the system without the suitable concentrations of TG which makes the efficiency of the transesterification process depend only on the concentration of TG. Therefore, the occurred transesterification reactions for spent SFO over S-CB appear to follow the pseudo-first-order kinetic properties as in eq 6.[34]

$$-\ln(1 - Y_{ME}) = kt \quad (6)$$

The kinetic properties were addressed considering the methanol/SFO ratio and S-CB loading at their best values of 15/1 and 3.5 wt %, respectively. The reactions intervals were assessed from 20 min up to 100 min and the transesterification temperature from 50 °C up to 70 °C. The high determination coefficient of the fitting processes for all the tests which were conducted at different temperature values ($C^2 > 0.95$) suggests a kinetic behavior of pseudo-first order properties and adsorption-surface reaction-desorption as an effective mechanism[3] (Figure 7A; Table S2). The value of the activation energy was determined theoretically according to the Arrhenius equation (eq 7) considering the regression fitting results of ln k versus $1/T$ as in eq 8. The estimated value (15.39 kJ/mol) reflects the possible performing of transesterification reactions at mild conditions and low energy[33] (Figure 7B).

$$k = \exp\left(-\frac{E_a}{RT}\right) \quad (7)$$

$$\ln k = A\frac{-E_a}{RT} + \ln A \quad (8)$$

2.5. Suggested Mechanism. The sulfonation process of CB can be illustrated based on its composition. The CB composed of inorganic aluminosilicate layers intercalated with organic kerogen. During the interaction between H_2SO_4 and the interlayer kerogen, the present sulfur ions and their trioxide species attack the aromatic rings of kerogen causing destruction for their double bonds and incorporation for the active acidic $-SO_3H$ group[35,36] (Figure 8). Additionally, the other oxidation effect occurs for the hydroxyl groups which

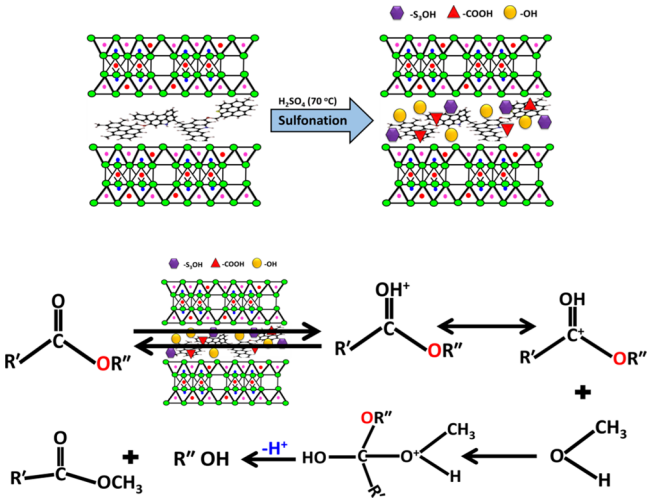

Figure 8. Schematic diagram for the formation mechanism of the S-CB acidic catalyst and the transesterification of spent sunflower it over it.

cause alteration of them to active carboxyl groups (COOH).[36,37] For the aluminosilicate layers, the reaction with H_2SO_4 causes modification for their surface with acidic sulfate anions which are attached to the surface by inner-sphere and outer-sphere complexes.[25]

Generally, the transesterification process involved reaction between the TGs of the vegetable oils and the used alcohol molecules creating monoesters is the existence of the used catalyst (S-CB) (Figure 8). The occurred reaction includes hydrolysis processes for the ester groups between the GR and the fatty acids.[1] This resulted in new types of ester bonds between the alcohol molecules and the fatty acids followed by replacement effect for the present GR by three monohydric alcohols. The suggested mechanism for the transesterification reaction of spent SFO over S-CB as an acidic catalyst as well as the predicted nucleophilic attacks of the ester groups was presented schematically in Figure 8.[14]

2.6. Comparison Study. The performance of the synthetic S-CB catalyst during the transesterification of the SFO was compared with other studied acidic catalysts considering the transesterification parameters (Table 5). The catalyst shows

https://doi.org/10.1021/acsomega.1c05021
ACS Omega 2021, 6, 31260−31271

Table 5. Comparing the Efficiency of the Synthetic S.CB with Other Acidic and Basic Catalysts in Literature

catalyst	time	temperature (°C)	methanol to oil	dosage (wt %)	yield (%)	references
sulfonated carbon	1 h	65	15:1	4	97	13
sulfonated graphene	14 h	100	20:1	10	98	38
$SO_4/Fe-Al-TiO_2$	2.5	90	10:1	3	96	39
$Fe_2O_3-MnO-SO_4/ZrO_2$	6 h	180	20:1	3	96	40
$Ti(SO_4)O$	3 h	75	9:1	1.5	97	41
sulfonated carbon	8 h	65	12:1	0.25	95	42
sulfonated AC from bamboo	3 h	85	7:1	12	96	43
S.CB (theoretical)	98 min	62	14.4:1	3.4	97.9	this study
S.CB (experimental)	85 min	50	15:1	3.5	96	this study

higher yields than some synthetic catalysts as $SO_4/Fe-Al-TiO_2$, $Fe_2O_3-MnO-SO_4/ZrO_2$, and $Ti(SO_4)O$ and values close to the synthetic sulfonated graphene (Table 5). This gives preferences for the synthetic S-CB catalyst considering the cost and the simplicity of the production processes.

4. CONCLUSIONS

CB was successfully treated by sulfonation reaction producing an acidic catalyst functionalized with $-SO_3H$ (S-CB) for effective transesterification of spent SFO. The catalytic activity was assessed considering series of random tests suggested by a statistical design (CCRD). The catalyst is of promising activity to achieve 96% as biodiesel yield at experimental conditions of 85 min at reaction interval, 50 °C as temperature, 15:1 as methanol/oil ratio, and 3.5 wt % as S-CB loading. Theoretically, the activity of the S-CB catalyst can be enhanced to achieve 97.9% yield by adjusting the values of temperature at 62 °C, the time at 98.5 min, the methanol/SFO ratio at 14.4:1, and S-CB loading at 3.4 wt %. The occurred SFO transesterification reactions over S-CB are of pseudo-first order kinetic and of low activation energy. The S-CB acidic catalyst is a recyclable product and the resulted biodiesel over it is of acceptable technical properties at biofuel.

5. EXPERIMENTAL WORK

5.1. Materials. The studied CB was collected as mining byproducts from Abu-Tartur phosphate mine, Western Desert, Egypt. The studied CB sample is 2.76% total organic carbon (TOC) is confirming intercalation of the bentonite layers with the organic matters. The studied CB sample composed essentially of 54.1% SiO_2, 24.73% Al_2O_3, 6.02% Fe_2O_3, 1.09% MgO, 1.78% SO_3, 0.09% Na_2O, 1.12% K_2O, 0.5% Cl, and 10.57% loss of ignition. Sulfuric acid of analytical grade (98% purity; Sigma-Aldrich; Egypt) was used in the sulfonation reactions of CB. SFO and methanol (99.8% purity; Sigma-Aldrich Egypt) were incorporated as the liquid phases during the transesterification experiments. The physical and chemical properties of the used SFO were presented in Table S3.

5.2. Sulfonation of Carbonaceous Bentonite. The sulfonation conditions were selected after series of primarily tests considering the influence of the acid concentration, the sulfonation time, and the sulfonation temperature. The CB samples were first crushed and ground by a ball mill to reduce the size of their fragments to less than 100 μm. After that, 50 g of the ground CB was dispersed homogeneously within 250 mL of sulfuric acid (70%) at a certain temperature of 10 °C for 120 min as acidification time at the inert environment of the nitrogen atmosphere. Then, the mixture was cooled down to room temperature, and then the acidified CB solid fractions were separated by filtration using a Whatman filter paper (45 μm) and washed carefully using distilled water for more than five runs until attaining the neutral pH. Finally, the sulfonated bentonite sample was dried at 75 °C for 4 h and then the product (S-CB) was kept for the next characterization and application steps.

5.3. Characterization Techniques. The XRD patterns of CB and S-CB were studied using a PANalytical X-ray diffractometer (Empyrean) of Cu Kα radiation to investigate the expected changes in the crystalline properties with the sulfonation process. The petrographic features of the raw CB sample in its thin sections were studied utilizing a Nikon polarizing transmitted microscope. The surface features and morphologies before and after the sulfonation processes were studied based on their SEM images using SEM (Gemini, Zeiss-Ultra 55) within accelerating voltage from about 5 kV up to 30 kV. Additionally, the EDX (energy dispersive X-ray spectroscopy) was applied to estimate the elemental compositions of CB, S-CB, and the used S-CB catalyst.

The sulfonation effect on the chemical structure of CB was assessed based on the FT-IR spectra of the materials using FT-IR spectrometer (FTIR-8400S; Shimadzu). The measuring process of the spectra was conducted at 37° as scan, 4 cm^{-1} as resolution, and frequency range from 400 cm^{-1} up to 4000 cm^{-1}. Prior to the determination, the powder of CB, S-CB, and the used S-CB were mixed with KBr (Merck) at a ratio of 1:10 to obtain translucent pellets which were used to identify the functional groups.

The surface area of both CB and S-CB was determined using a surface area analyzer (Beckman Coulter SA3100) based on their N_2 adsorption/desorption isotherm curves which were treated with BJH method for the porosity and Brunauer–Emmett–Teller method for the surface area. The measuring processes were performed after degassing of the materials at 100 °C for 2 h under vacuum and determination temperature was adjusted at 77 K.

The densities of the essential acid groups were measured considering the Boehm titration method. About 0.5 g of the S-CB catalyst was mixed with solutions of Na_2CO_3 (0.05 M; 17 mL), $NaHCO_3$ (0.05 M; 17 mL), Na_2SO_4 (1.0 M; 20 mL), and NaOH (0.05 M; 17 mL). Then, the produced mixtures were stirred for about 24 h and this was followed by separation of the S-CB particles by filtration. Then, about 5 mL of extracted four aliquot solutions was treated with diluted HCl (0.05 M) before determining of the main acidic groups by a simple titration method utilizing NaOH solution (0.05 M) and an indicator of phenolphthalein.

5.4. Transesterification System. The transesterification of the spent SFO over the S-CB acidic catalyst was carried out using an autoclave of Teflon (150 mL) as a closed

https://doi.org/10.1021/acsomega.1c05021
ACS Omega 2021, 6, 31260−31271

transformation reactor. A digital magnetic stirrer was used to homogenize the incorporated reactant with each other considering the speed at 500 rpm and the transesterification temperature was adjusted using the attached digital hot plate. The essential factors that were evaluated as the control parameters for the experiments are the reaction time (min), the methanol content (molar ratio), the temperature (°C), and the incorporated S-CB loading (wt %). The adjusted values for all the studied factors were selected based on the suggested conditions by the built statistical CCR design in conjunction with the RSM. Design-Expert software (Version 6.0.5) is the used software to build the design and to assess the influence of the affected factors and the recognized results. The values of the factors as inputs were selected considering the obtained results for series of primarily tests which were conducted for each factor separately and the lower levels for the influence of the factors were selected at the values which achieve 50% biodiesel yield. The selected lower and upper values for all the studied experimental factors are listed in Table S4 either in their coded values or their real values.

The experimental procedures involved as a first step the careful, filtration of the spent SFO to isolate the solid suspensions. After that, 40 g of the SFO was heated at about 75 °C for 20 min as a required step to avoid the effect of the humidity or the moisture content. Then, the S-CB catalyst (with 15−100 μm particle size) was added at a certain loading based on the suggested value by the design and mixed with the oil for about 10 min. This followed by the addition of the alcohol at its suggested ratio to the SFO. Finally, the reactants were left under stirring for certain periods and at adjusted temperature according to suggested conditions of the followed design.

By ending the tests according to the statistically suggested conditions, the solid particles of the S-CB catalyst were extracted from the converted SFO by centrifugation at a fixed speed of 3500 rpm. Then, the converted SFO samples were transferred into separating funnels of glass and all the samples were left for about 24 h as an essential step to confirm the complete settle down of the present GR molecules as dense layers at the bottoms of the funnels to be removed easily from the formed biodiesel based SFO. The resulted biodiesel as products for the transesterification of the spent SFO was heated for 5 h at about 85 °C to avoid the effect of any residuals for free alcohol molecules. The determination of the generated FAME in the converted SFO samples was conducted using a gas-chromatography technique (Agilent 7890A) after the dilution process using *n*-hexane and using an internal standard of methyl heptadecanoate. The biodiesel yields were calculated considering the measured FAME content according to eq 9.

$$\text{biodiesel yield (\%)} = \frac{(\text{weight of biodiesel } x \text{ \% FAME})}{\text{weight of oil}} \times 100 \quad (9)$$

Considering the second-order polynomial model as the descriptive model for the studied S-CB transesterification reaction for spent SFO, the illustrative equation for the influence of the factors as inputs and achieved biodiesel yield as the response can be represented by eq 10.

$$Y = \beta_o + \sum_{i=1}^{k} \beta_i X_i + \sum_{i=1}^{k} \beta_{ii} X_i^2 + \sum_{i=1}^{k-1} \sum_{j=i+1}^{k} \beta_{ij} X_i X_j \quad (10)$$

The presented symbols in the equations refer to biodiesel yield (Y), input parameters (X_i and X_j), constant (β_0), coefficient linear term (β_i), coefficient quadratic term (β_{ii}), coefficient cross-product term (β_{ij}), and the number of the factors (K).

■ ASSOCIATED CONTENT

Supporting Information

The Supporting Information is available free of charge at https://pubs.acs.org/doi/10.1021/acsomega.1c05021.

Petrographic properties of the studied CB sample , SEM images of the spent S-CB catalyst , normal probability plot for studentized residuals , optimization test scheme constraints for the optimizing solutions , determination coefficient and the rate constant of pseudo-first order kinetic model, fatty acid composition and physical properties of SFO, and values of the inserted variables in the statistical design (PDF)

■ AUTHOR INFORMATION

Corresponding Author

Mostafa R. Abukhadra − *Geology Department, Faculty of Science and Materials Technologies and Their Applications Lab, Geology Department, Faculty of Science, Beni-Suef University, Beni Suef 62511, Egypt;* orcid.org/0000-0001-5404-7996; Email: Abukhadra89@Science.bsu.edu.eg

Authors

Walaa A. Hassan − *Geology Department, Faculty of Science, Assiut University, Assiut 71515, Egypt*

Ezzat A. Ahmed − *Geology Department, Faculty of Science, Assiut University, Assiut 71515, Egypt*

Mohamed A. Moneim − *Geology Department, Faculty of Science, Assiut University, Assiut 71515, Egypt*

Mohamed S. Shaban − *Geology Department, Faculty of Science, New Valley University, El-Kharga 72511, Egypt*

Ahmed M. El-Sherbeeny − *Industrial Engineering Department, College of Engineering, King Saud University, Riyadh 11421, Saudi Arabia*

Nahid Siddiqui − *Amity Institute of Biotechnology, Amity University, Noida 201301, India*

Jae-Jin Shim − *School of Chemical Engineering, Yeungnam University, Gyeongsan 38541, Republic of Korea*

Complete contact information is available at: https://pubs.acs.org/10.1021/acsomega.1c05021

Author Contributions

This article was written through the contributions of all authors. All authors have given approval to the final version of the manuscript

Notes

The authors declare no competing financial interest.

■ ACKNOWLEDGMENTS

The authors extend their appreciation to Assiut University for supporting the study. Additionally, the authors extend their appreciation to King Saud University for funding this work

through researchers supporting project number (RSP-2021/133), King Saud University, Riyadh, Saudi Arabia.

REFERENCES

(1) Basyouny, M. G.; Abukhadra, M. R.; Alkhaledi, K.; El-Sherbeeny, A. M.; El-Meligy, M. A.; Soliman, A. T. A.; Luqman, M. Insight into the catalytic transformation of the waste products of some edible oils (corn oil and palm oil) into biodiesel using MgO/clinoptilolite green nanocomposite. *Mol. Catal.* **2021**, *500*, 111340.

(2) Lee, J. H.; Jeon, H.; Park, J. T.; Kim, J. H. Synthesis of hierarchical flower-shaped hollow MgO microspheres via ethylene-glycol-mediated process as a base heterogeneous catalyst for transesterification for biodiesel production. *Biomass Bioenergy* **2020**, *142*, 105788.

(3) Li, Z.; Ding, S.; Chen, C.; Qu, S.; Du, L.; Lu, J.; Ding, J. Recyclable Li/NaY zeolite as a heterogeneous alkaline catalyst for biodiesel production: Process optimization and kinetics study. *Energy Convers. Manag.* **2019**, *192*, 335−345.

(4) Lawan, I.; Garba, Z. N.; Zhou, W.; Zhang, M.; Yuan, Z. Synergies between the microwave reactor and CaO/zeolite catalyst in waste lard biodiesel production. *Renew. Energy* **2020**, *145*, 2550−2560.

(5) Zhong, L.; Feng, Y.; Wang, G.; Wang, Z.; Bilal, M.; Lv, H.; Jia, S.; Cui, J. Production and use of immobilized lipases in/on nanomaterials: A review from the waste to biodiesel production. *Int. J. Biol. Macromol.* **2020**, *152*, 207−222.

(6) Abukhadra, M. R.; Basyouny, M. G.; El-Sherbeeny, A. M.; El-Meligy, M. A.; Luqman, M. Insights into the green doping of clinoptilolite with Na^+ ions (Na^+/Clino) as a nanocatalyst in the conversion of palm oil into biodiesel; optimization and mechanism. *Nanotechnology* **2021**, *32*, 155702.

(7) Ibrahim, M. L.; Nik Abdul Khalil, N. N. A.; Islam, A.; Rashid, U.; Ibrahim, S. F.; Sinar Mashuri, S. I.; Taufiq-Yap, Y. H. Preparation of Na_2O supported CNTs nanocatalyst for efficient biodiesel production from waste-oil. *Energy Convers. Manag.* **2020**, *205*, 112445.

(8) Al Hatrooshi, A. S.; Eze, V. C.; Harvey, A. P. Production of biodiesel from waste shark liver oil for biofuel applications. *Renew. Energy* **2020**, *145*, 99−105.

(9) Mohadesi, M.; Aghel, B.; Maleki, M.; Ansari, A. The use of KOH/Clinoptilolite catalyst in pilot of microreactor for biodiesel production from waste cooking oil. *Fuel* **2020**, *263*, 116659.

(10) Sayed, M. R.; Abukhadra, M. R.; Abdelkader Ahmed, S.; Shaban, M.; Javed, U.; Betiha, M. A.; Shim, J.-J.; Rabie, A. M. Synthesis of advanced MgAl-LDH based geopolymer as a potential catalyst in the conversion of waste sunflower oil into biodiesel: response surface studies. *Fuel* **2020**, *282*, 118865.

(11) Melero, J. A.; Iglesias, J.; Morales, G. Heterogeneous acid catalysts for biodiesel production: current status and future challenges. *Green Chem.* **2009**, *11*, 1285−1308.

(12) Wang, Y.-T.; Yang, X.-X.; Xu, J.; Wang, H.-L.; Wang, Z.-B.; Zhang, L.; Wang, S.-L.; Liang, J.-L. Biodiesel production from esterification of oleic acid by a sulfonated magnetic solid acid catalyst. *Renew. Energy* **2019**, *139*, 688−695.

(13) Farabi, M. S. A.; Ibrahim, M. L.; Rashid, U.; Taufiq-Yap, Y. H. Esterification of palm fatty acid distillate using sulfonated carbon-based catalyst derived from palm kernel shell and bamboo. *Energy Convers. Manag.* **2019**, *181*, 562−570.

(14) Betiha, M. A.; Negm, N. A.; El-Sayed, E. M.; Mostafa, M. S.; Menoufy, M. F. Capability of synthesized sulfonated aromatic cross-linked polymer covalently bonded montmorillonite framework in productivity process of biodiesel. *J. Clean. Prod.* **2020**, *261*, 120995.

(15) Negm, N. A.; Sayed, G. H.; Yehia, F. Z.; Habib, O. I.; Mohamed, E. A. Biodiesel production from one-step heterogeneous catalyzed process of Castor oil and Jatropha oil using novel sulphonated phenyl silane montmorillonite catalyst. *J. Mol. Liq.* **2017**, *234*, 157−163.

(16) Flores, K. P.; Omega, J. L. O.; Cabatingan, L. K.; Go, A. W.; Agapay, R. C.; Ju, Y.-H. Simultaneously carbonized and sulfonated sugarcane bagasse as solid acid catalyst for the esterification of oleic acid with methanol. *Renew. Energy* **2019**, *130*, 510−523.

(17) Shi, Y.; Kevin, M.-W.; Liang, X. Facile synthesis of novel porous carbon based solid acid with microtube structure and its catalytic activities for biodiesel synthesis. *J. Environ. Chem. Eng.* **2018**, *6*, 6633−6640.

(18) Aniya, V.; Kumari, A.; De, D.; Vidya, D.; Swapna, V.; Thella, P. K.; Satyavathi, B. Translation of lignocellulosic waste to mesoporous solid acid catalyst and its efficacy in esterification of volatile fatty acid. *Microporous Mesoporous Mater.* **2018**, *264*, 198−207.

(19) Abdel Salam, M.; Abukhadra, M. R.; Adlii, A. Insight into the Adsorption and Photocatalytic Behaviors of an Organo-bentonite/Co_3O_4 Green Nanocomposite for Malachite Green Synthetic Dye and Cr (VI) Metal Ions: Application and Mechanisms. *ACS Omega* **2020**, *5*, 2766.

(20) Dardir, F. M.; Mohamed, A. S.; Abukhadra, M. R.; Ahmed, E. A.; Soliman, M. F. Cosmetic and pharmaceutical qualifications of Egyptian bentonite and its suitability as drug carrier for Praziquantel drug. *Eur. J. Pharm. Sci.* **2018**, *115*, 320−329.

(21) De Mattos Amadio, T.; Hotza, D.; Batista Rodrigues Neto, J.; Blosi, M.; Costa, A. L.; Dondi, M. Bentonites functionalized by impregnation with TiO_2, Ag, Pd and Au nanoparticles. *Appl. Clay Sci.* **2017**, *146*, 1−6.

(22) Abukhadra, M. R.; Shaban, M.; Sayed, F.; Saad, I. Efficient photocatalytic removal of safarnin-O dye pollutants from water under sunlight using synthetic bentonite/polyaniline@ Ni_2O_3 photocatalyst of enhanced properties. *Environ. Sci. Pollut. Res.* **2018**, *25*, 33264−33276.

(23) Abukhadra, M. R. Evaluation of Egyptian oil shale as alternative source of energy. *Academic J. App. Sci. Res.* **2016**, *1*, 11.

(24) Sobhy, A.; Yehia, A.; Hosiny, F. I. E.; Ibrahim, S. S.; Amin, R. Application of statistical analysis for optimizing of column flotation with pine oil for oil shale cleaning. *Int. J. Coal Prep. Util.* **2020**, 1−14.

(25) Shaban, M.; Abukhadra, M. R.; Khan, A. A. P.; Jibali, B. M. Removal of Congo red, methylene blue and Cr (VI) ions from water using natural serpentine. *J. Taiwan Inst. Chem. Eng.* **2018**, *82*, 102−116.

(26) Shaban, M.; Abukhadra, M. R.; Shahien, M. G.; Khan, A. A. P. Upgraded modified forms of bituminous coal for the removal of safranin-T dye from aqueous solution. *Environ. Sci. Pollut. Res.* **2017**, *24*, 18135−18151.

(27) Akinfalabi, S.-I.; Rashid, U.; Yunus, R.; Taufiq-Yap, Y. H. Synthesis of biodiesel from palm fatty acid distillate using sulfonated palm seed cake catalyst. *Renew. Energy* **2017**, *111*, 611−619.

(28) Toledo Arana, J.; Torres, J. J.; Acevedo, D. F.; Illanes, C. O.; Ochoa, N. A.; Pagliero, C. L. One-step synthesis of CaO-ZnO efficient catalyst for biodiesel production. *Int. J. Chem. Eng.* **2019**, 1806017.

(29) Seela, C. R.; Alagumalai, A.; Pugazhendhi, A. Evaluating the feasibility of diethyl ether and isobutanol added Jatropha Curcas biodiesel as environmentally friendly fuel blends. *Sustain. Chem. Pharm.* **2020**, *18*, 100340.

(30) Rabie, A. M.; Shaban, M.; Abukhadra, M. R.; Hosny, R.; Ahmed, S. A.; Negm, N. A. Diatomite supported by CaO/MgO nanocomposite as heterogeneous catalyst for biodiesel production from waste cooking oil. *J. Mol. Liq.* **2019**, *279*, 224−231.

(31) Abukhadra, M. R.; Mohamed, A. S.; El-Sherbeeny, A. M.; Soliman, A. T. A.; Abd Elgawad, A. E. E. Sonication induced transesterification of castor oil into biodiesel in the presence of MgO/CaO nanorods as a novel basic catalyst: Characterization and optimization. *Chem. Eng. Process.* **2020**, *154*, 108024.

(32) Bhatia, S. K.; Gurav, R.; Choi, T.-R.; Kim, H. J.; Yang, S.-Y.; Song, H.-S.; Park, J. Y.; Park, Y.-L.; Han, Y.-H.; Choi, Y.-K.; Kim, S.-H.; Yoon, J.-J.; Yang, Y.-H. Conversion of waste cooking oil into biodiesel using heterogenous catalyst derived from cork biochar Bioresour. *Technol* **2020**, *302*, 122872.

(33) Naeem, A.; Wali Khan, I.; Farooq, M.; Mahmood, T.; Ud Din, I.; Ali Ghazi, Z.; Saeed, T. Kinetic and optimization study of sustainable biodiesel production from waste cooking oil using novel

https://doi.org/10.1021/acsomega.1c05021
ACS Omega 2021, 6, 31260−31271

heterogeneous solid base catalyst. *Bioresour. Technol.* **2021**, *328*, 124831.
(34) Roy, T.; Sahani, S.; Madhu, D.; Chandra Sharma, Y. A clean approach of biodiesel production from waste cooking oil by using single phase $BaSnO_3$ as solid base catalyst: Mechanism, kinetics & E-study. *J. Clean. Prod.* **2020**, *265*, 121440.
(35) Xiao, Y.; Hill, J. M. Solid acid catalysts produced by sulfonation of petroleum coke: Dominant role of aromatic hydrogen. *Chemosphere* **2020**, *248*, 125981.
(36) Tang, X.; Niu, S.; Zhao, S.; Zhang, X.; Li, X.; Yu, H.; Lu, C.; Han, K. Synthesis of sulfonated catalyst from bituminous coal to catalyze esterification for biodiesel production with promoted mechanism analysis. *J. Ind. Eng. Chem.* **2019**, *77*, 432−440.
(37) Yu, H.; Niu, S.; Bai, T.; Tang, X.; Lu, C. Microwave-assisted preparation of coal-based heterogeneous acid catalyst and its catalytic performance in esterification. *J. Clean. Prod.* **2018**, *183*, 67−76.
(38) Nongbe, M. C.; Ekou, T.; Ekou, L.; Yao, K. B.; Le Grognec, E.; Felpin, F.-X. Biodiesel production from palm oil using sulfonated graphene catalyst. *Renew. Energy* **2017**, *106*, 135.
(39) Gardy, J.; Osatiashtiani, A.; Céspedes, O.; Hassanpour, A.; Lai, X.; Lee, A. F.; Wilson, K.; Rehan, M. A magnetically separable SO_4/Fe-Al-TiO_2 solid acid catalyst for biodiesel production from waste cooking oil. *Appl. Catal., B* **2018**, *234*, 268−278.
(40) Alhassan, F. H.; Rashid, U.; Taufiq-Yap, Y. H. Synthesis of waste cooking oil-based biodiesel via effectual recyclable bi-functional Fe_2O_3-MnO-SO_4^{2-}/ZrO_2 nanoparticle solid catalyst. *Fuel* **2015**, *142*, 38−45.
(41) Gardy, J.; Hassanpour, A.; Lai, X.; Ahmed, M. H. Synthesis of $Ti(SO_4)O$ solid acid nano-catalyst and its application for biodiesel production from used cooking oil. *Appl. Catal., A* **2016**, *527*, 81−95.
(42) Zhang, H.; Luo, X.; Li, X.; Chen, G. Z.; He, F.; Wu, T. Preparation and Characterization of a Sulfonated Carbon-based Solid Acid Microspheric Material (SCSAM) and its use for the Esterification of Oleic Acid with Methanol. *Austin Chem. Eng.* **2016**, *3*, 1024.
(43) Niu, S.; Ning, Y.; Lu, C.; Han, K.; Yu, H.; Zhou, Y. Esterification of oleic acid to produce biodiesel catalyzed by sulfonated activated carbon from bamboo. *Energy Convers. Manag.* **2018**, *163*, 59−65.

https://doi.org/10.1021/acsomega.1c05021
ACS Omega 2021, 6, 31260−31271